UDC 539.3 **doi: 10.32620/aktt.2026.3.04**

Ihor ARKHYPENKO

National Aerospace University «Kharkiv Aviation Institute», Kharkiv, Ukraine

STRESS STATE ANALYSIS OF SEMI-INFINITE LAYER WITH CYLINDRICAL CAVITIES

The subject matter of the article is *the stress-strain state of a semi-bounded isotropic elastic layer with N longitudinal cylindrical cavities under prescribed displacements on all surfaces of the body.* ***The goal is*** *to develop an analytical-numerical methodology for solving the spatial elasticity problem for the semi-bounded layer with cylindrical cavities under kinematic boundary conditions and to investigate the stress state for four qualitatively distinct variants of boundary conditions differing in the parity of the prescribed displacement components with respect to the coordinate z.* ***The tasks to be solved are*** *as follows: to construct a solution of the Lamé equations in Cartesian and local cylindrical coordinate systems; to reduce the problem for the semi-bounded layer to an equivalent problem for an infinite layer; to satisfy the boundary conditions on all surfaces and reduce the problem to an infinite system of linear algebraic equations; to obtain numerical stress distributions on the layer boundaries and cavity surfaces; to verify the methodology against known solutions.* ***The methods used are*** *the generalized Fourier method with addition theorems for transition between coordinate systems; the mirror reflection method, whereby assigning even or odd displacements on the horizontal boundaries automatically enforces «smooth wall» or «free face» conditions on the plane z = 0; and the reduction method for solving the resulting infinite system of linear algebraic equations of the second kind.* ***Conclusions.*** *Even-parity loadings give rise to nearly the full set of stress components in the cross-section of the cavity, whereas odd-parity loadings produce a predominantly antiplane stress state. Normal displacement produces stress concentration on the cavity surface 3.5–4 times greater than the tangential displacement of the same amplitude. An oscillatory stress distribution near the discontinuity points of the prescribed displacements is of a physical nature and is independent of the truncation order of the system.* ***Scientific novelty.*** *For the first time, the spatial elasticity problem for a semi-bounded layer with N cylindrical cavities under kinematic boundary conditions has been solved. The combination of the generalized Fourier method with the mirror reflection method is extended to a semi-bounded body with cylindrical inhomogeneity. The methodology is applicable to an arbitrary number of cavities and may serve as a benchmark for verification of finite element solutions.*

Keywords: *semi-infinite layer; cylindrical cavity; kinematic boundary conditions; generalized Fourier method; stress-strain state; spatial edge effect.*

Introduction

The development of modern aerospace technology imposes increasingly stringent requirements for the accuracy of strength calculations of structural elements of aviation and rocket-space systems. Fuselage panels, wing stringers, frames, elements of power units and control aggregates contain numerous structural holes, technological channels, pneumatic and hydraulic pipelines, which are sources of stress concentration. Under cyclic loading, a wide range of operating temperatures and vibrational influences, most fatigue cracks initiate precisely in stress concentration zones, determining the resource and reliability of the structure. Therefore, an accurate determination of the stress-strain state (SSS) near cylindrical channels and holes is a critically important scientific and practical design task for aviation structures.

This problem becomes particularly relevant when calculating parts subjected to forced deformation - clamping in rigid joints, thermal deformations, interference fit deformations. In such cases, displacements rather than forces are specified at the body boundaries, corresponding to kinematic boundary conditions. Despite the widespread occurrence of such structural situations, elasticity theory problems with kinematic boundary conditions for bodies with cylindrical cavities are significantly less studied than analogous problems with force conditions.

An additional source of complexity is the semi-infinity of structural elements: most real aviation parts have end surfaces where edge effects arise, significantly affecting the stress distribution near cylindrical concentrators. Meanwhile, the majority of theoretical studies focus on infinite or unbounded bodies, and results from these works cannot be directly applied to the calculation of finite structural elements.

Thus, the problem of SSS in a semi-infinite layer with cylindrical cavities under kinematic boundary conditions is relevant both theoretically and practically: its solution fills the existing gap in elasticity theory and provides aerospace engineers with a reliable analytical-numerical tool for assessing stress concentration in critical

ISSN 1814-4225 (print)
ISSN 2663-2012 (online)

structural elements.

1. State of the art

The fundamental foundations of the theory of stress concentration around holes in elastic bodies are laid out in Savin's monograph [1], where plane problems for bodies with holes of various shapes are systematized. Three-dimensional problems of the theory of elasticity for bodies with cylindrical boundaries are considered in the monographs of Kosmodamiansky [2] and Podilchuk [3]; however, these works do not consider the case of a layer with a vertical boundary. Harmonic oscillations and waves in elastic bodies with cylindrical inhomogeneities were studied in the monograph by Grinchenko and Meleshko [4], but static problems for semi-infinite regions are not considered there. For practical calculations, numerical approaches are widely used — the finite element method and corresponding software packages [5, 6]. However, they do not provide analytical relationships for parametric analysis and require verification.

A powerful analytical tool is the generalized Fourier method, systematically developed in the monograph by Nikolaev and Protsenko [7]. In this work, basis solutions of the Lamé equations and addition theorems for transitioning between Cartesian and cylindrical coordinate systems are constructed; however, problems for a semi-infinite layer are not considered there. Fesenko and Vaisfeld [8, 9] applied the generalized Fourier method to dynamic problems for an infinite layer with a transverse cylindrical cavity, investigating wave processes and diffraction of elastic waves. Despite the effectiveness of this approach for dynamic problems, static problems with kinematic boundary conditions for a layer with a vertical end and parallel cylindrical cavities are not considered in works [8, 9]. Stress concentration around circular holes in functionally graded plates under various types of loading was investigated in the work of Khechai et al. [10], but the problem for a layer with a vertical end is not posed there.

Static problems for an infinite layer with cylindrical cavities under prescribed stresses on flat boundaries have been studied in a series of works. Miroshnikov et al. [11] solved the second fundamental problem (in displacements) for a layer with one cavity, [12] — for a layer with a cavity under periodic loading. Nikichanov [13] considered the problem for a layer with a cavity under conditions of smooth contact on flat boundaries and prescribed displacements on the cavity surface, however, the layer in this work is infinite and only one cavity is considered. Miroshnikov et al. [14] generalized the problem to the case of N cylindrical cavities, but again for an infinite layer and only for force boundary conditions. Problems with elastic inclusions in the form of pipes were investigated in works [15–19], where rotation conditions [15], hinged joints [16], thick-walled pipes [17], rigid clamping [18], and combined contact conditions [19] were considered. However, in all these works [15–19] the layer is infinite.

Thus, the problem for a semi-infinite layer with cylindrical inhomogeneities is only beginning to be investigated. Arkhypenko and Savin in works [20, 21] proposed a concept for solving the problem of elasticity theory for a semi-infinite layer using the method of mirror images: prescribing even or odd loads on the boundaries of an equivalent infinite layer allows modeling the "smooth wall" or "free end" conditions on the plane z = 0 without directly introducing this boundary. In work [22] this direction is developed for a semi-infinite layer with one cylindrical cavity and a cylindrical pipe. However, in both works [20, 21], cylindrical inhomogeneities are absent, and in work [22] the problem is considered only for two inhomogeneities and in stresses.

Therefore, the problem for a semi-infinite layer with N cylindrical cavities under kinematic boundary conditions (prescribed displacements) on all body surfaces remains unsolved. It is the combination of the semi-infiniteness of the layer with a vertical end, an arbitrary number of cylindrical cavities, and boundary conditions in displacements (symmetric and antisymmetric) that forms a qualitatively new mathematical problem that has not been previously considered in the literature.

The aim of this work is to develop an analytical-numerical methodology and investigate the stress state of a semi-infinite elastic layer with N longitudinal cylindrical cavities under prescribed displacements on all surfaces of the body, taking into account the "smooth wall" and "free end" conditions on the vertical end z = 0.

2. Materials and methods of research

2.1. Formulation of the Research Problem

In the Cartesian coordinate system (x, y, z), an isotropic elastic layer with modulus of elasticity E and Poisson's ratio ν, bounded by horizontal planes $y = h$ and $y = -h$ and a vertical end z=0 (Fig. 1) is considered. Inside the layer along the axis z parallel to its horizontal boundaries, N cylindrical cavities of radii R_p (p=1,…,N) are located. The centers of the cavity cross-sections are located at points (x_p, y_p).

The stress-strain state of the layer is described by the vector Lamé equation in displacements:

$$(1-2\nu)\Delta\vec{U} + \text{grad div}\,\vec{U} = 0 \qquad (1)$$

where $\vec{U} = \left(u_x, u_y, u_z\right)$ is the displacement vector, ν — Poisson's ratio, Δ is the Laplace operator. This equation

is valid for every point of the layer outside the cylindrical cavities.

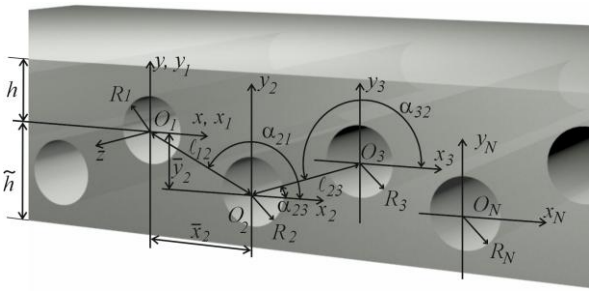

Fig. 1. Semi-infinite layer with cylindrical cavities

On the horizontal boundaries of the layer, displacements are prescribed. Four independent variants of non-zero boundary conditions that differ in the parity of functions with respect to coordinate z are considered:

Variant 1 (u_y even in z — condition of a "smooth wall"):

$$u_y(x,h,z) = u_y(x,h,-z) \tag{2}$$

Variant 2 (u_x even in z — condition of a "smooth wall"):

$$u_x(x,h,z) = u_x(x,h,-z) \tag{3}$$

Variant 3 (u_y odd in z — condition of a "free end"):

$$u_y(x,h,z) = -u_y(x,h,-z) \tag{4}$$

Variant 4 (u_x odd in z — condition of a "free end"):

$$u_x(x,h,z) = -u_x(x,h,-z) \tag{5}$$

All prescribed functions are rapidly decaying as $|x|\to\infty$ and $|z|\to\infty$.

On the surface of each cylindrical cavity ($\rho_p=R_p$, p=1,…,N), displacements are prescribed:

$$\vec{U}\big|_{\rho_p=R_p} = \vec{f}^{(p)}(\varphi_p, z) \tag{6}$$

where ρ_p, φ_p are polar coordinates in a local cylindrical system centered on the axis of the p-th cavity, $\vec{f}^{(p)}$ is the prescribed displacement vector function.

A key feature of the mathematical model is the approach to satisfying conditions on the vertical end z=0. Instead of directly solving the problem for a semi-infinite body, the mirror reflection method is applied [20 – 22]: an infinite layer is considered , on the horizontal boundaries of which even or odd (in z) displacements are prescribed. Due to the properties of symmetry and antisymmetry of the solution, the following conditions are automatically satisfied on the plane:

— "smooth wall" (variants 1, 2): absence of normal displacement and tangential stresses:

$$u_z\big|_{z=0} = 0,\ \tau_{xz}\big|_{z=0} = 0,\ \tau_{yz}\big|_{z=0} = 0 \tag{7}$$

— "free end" (variants 3, 4): absence of normal and tangential stresses:

$$\sigma_x\big|_{z=0} = 0,\ \sigma_y\big|_{z=0} = 0,\ \sigma_z\big|_{z=0} = 0, \tag{8}$$

Thus, the four variants of boundary conditions (2)–(5) generate four qualitatively different problems, which cover practically important deformation modes of a semi-infinite layer with N cylindrical cavities.

2.2. Solution method

To solve the boundary value problem (1)–(6), a set of analytical methods is applied, based on the generalized Fourier method [7] in combination with the mirror reflection method [20 – 22].

The displacement vector of the layer is sought in the form of a superposition of basis solutions of the Lamé equation in the Cartesian coordinate system and local cylindrical coordinate systems associated with each cavity [14]:

$$\vec{U}_1 = \sum_{k=1}^{3}\int_{-\infty}^{\infty}\int_{-\infty}^{\infty}\Big(H_k(\lambda,\mu)\cdot\vec{u}_k^{(+)}(x,y,z;\lambda,\mu) + \tilde{H}_k(\lambda,\mu)\cdot\vec{u}_k^{(-)}(x,y,z;\lambda,\mu)\,d\mu d\lambda\Big) + \sum_{p=1}^{3}\sum_{k=1}^{3}\int_{-\infty}^{\infty}\sum_{m=-\infty}^{\infty}B_{k,m}^{(p)}(\lambda)\cdot\vec{S}_{k,m}(\rho_p,\phi_p,z;\lambda)\,d\lambda \tag{9}$$

where $H_k(\lambda,\mu)$, $\tilde{H}_k(\lambda,\mu)$, $B_{k,m}^{(p)}(\lambda)$ – unknown functions (k = 1..3), which must be determined from the boundary conditions (2) – (6); $\vec{u}_k^{(+)}$, $\vec{u}_k^{(-)}$, $\vec{S}_{k,m}$, $\vec{R}_{k,m}$ – basis vector functions in Cartesian and cylindrical coordinate systems, which are presented in the form [7]

$$\vec{u}_k^{\pm}(x,y,z;\lambda,\mu) = N_k^{(d)}e^{i(\lambda z+\mu x)\pm\gamma y};$$

$$\vec{R}_{k,m}(\rho,\varphi,z;\lambda) = N_k^{(p)}I_m(\lambda\rho)e^{i(\lambda z+m\varphi)};$$

$$\vec{S}_{k,m}(\rho,\varphi,z;\lambda) = N_k^{(p)}\Big[(sign\lambda)^m K_m(|\lambda|\rho)\times e^{i(\lambda z+m\varphi)};$$

$k = 1, 2, 3;$

$$N_1^{(d)} = \frac{1}{\lambda}\nabla;\quad N_3^{(d)} = \frac{i}{\lambda}rot\left(\vec{e}_3^{(1)}\right);$$

$$N_2^{(d)} = \frac{4}{\lambda}(\nu-1)\vec{e}_2^{(1)} + \frac{1}{\lambda}\nabla(y);$$

$$N_1^{(p)} = \frac{1}{\lambda}\nabla;\quad N_3^{(p)} = \frac{i}{\lambda}rot\left(\vec{e}_3^{(2)}\right)$$

$$N_2^{(p)} = \frac{1}{\lambda}\left[\nabla\left(\rho\frac{\partial}{\partial\rho}\right) + 4(\nu-1)\left(\nabla - \vec{e}_3^{(2)}\frac{\partial}{\partial z}\right)\right];$$

$$\gamma = \sqrt{\lambda^2 + \mu^2},\ -\infty < \lambda, \mu < \infty$$

are modified Bessel functions.

According to the method of mirror reflection [20 – 22], the problem for a semi-infinite layer is reduced to a problem for an infinite layer by prescribing displacements with a certain parity in the coordinate *z* on the horizontal boundaries. For each of the four variants of boundary conditions (2)–(5), this ensures automatic fulfillment of conditions (7) or (8) on the plane z = 0, without introducing this boundary directly into the solution.

The evenness or oddness of the prescribed displacements in z determines the corresponding parity of spectral densities $H_k(\lambda,\mu)$, $\tilde{H}_k(\lambda,\mu)$ with respect to the parameter λ in the expansion (9), which significantly simplifies the structure of the system of equations.

Since boundary conditions are prescribed on surfaces described in different coordinate systems (planes y = ±h and cylinders $\rho_p = R_p$), addition theorems are applied to compare the basis solutions [7]:

– transition from external solutions for the cylinder $\vec{S}_{k,m}$ to solutions for the layer $\vec{u}_k^{(-)}$ (at y > 0) and $\vec{u}_k^{(+)}$ (at y < 0):

$$\vec{S}_{k,m}(\rho,\varphi,z;\lambda) = \frac{(-i)^m}{2}\int_{-\infty}^{\infty} \omega_{\mp}^m \cdot e^{-i\mu\bar{x}_p \pm \gamma\bar{y}_p} \times \times \vec{u}_k^{(\mp)} \cdot \frac{d\mu}{\gamma},\quad k = 1, 3; \tag{10}$$

$$\vec{S}_{2,m}(\rho,\varphi,z;\lambda) = \frac{(-i)^m}{2}\int_{-\infty}^{\infty} \omega_{\mp}^m \cdot \left(\left(\pm m\cdot\mu - \frac{\lambda^2}{\gamma} \pm \lambda^2 \bar{y}_p\right)\times \right.$$

$$\left. \times \vec{u}_1^{(\mp)} \mp \lambda^2 \vec{u}_2^{(\mp)} \pm 4\mu(1-\nu)\vec{u}_3^{(\mp)}\right)\frac{e^{-i\mu\bar{x}_p \pm \gamma\bar{y}_p}\, d\mu}{\gamma^2},$$

where $\bar{x}_p = \ell_{1p}\cos\alpha_{1p}$; $\bar{y}_p = \ell_{1p}\sin\alpha_{1p}$,

$\omega_{\mp}(\lambda,\mu) = \dfrac{\mu \mp \gamma}{\lambda}$, $m = 0, \pm1, \pm2, \ldots$.

– transition from solutions for the layer $\vec{u}_k^{(+)}$ and $\vec{u}_k^{(-)}$ to internal solutions for the $\vec{R}_{k,m}$:

$$\vec{u}_k^{(\pm)}(x,y,z) = e^{i\mu\bar{x}_p \pm \gamma\bar{y}_p} \cdot \sum_{m=-\infty}^{\infty} \left(i\cdot\omega_{\mp}\right)^m \vec{R}_{k,m},\quad (k = 1, 3); \tag{11}$$

$$\vec{u}_2^{(\pm)}(x,y,z) = e^{i\mu\bar{x}_p \pm \gamma\bar{y}_p} \cdot \sum_{m=-\infty}^{\infty} \left[\left(i\cdot\omega_{\mp}\right)^m \cdot \lambda^{-2} \times \right.$$

$$\left. \times \left(\left(m\cdot\mu + \lambda^2\bar{y}_p\right)\cdot\vec{R}_{1,m} \pm \gamma\cdot\vec{R}_{2,m} + 4\mu(1-\nu)\vec{R}_{3,m}\right)\right],$$

where $\vec{R}_{k,m} = \tilde{\vec{b}}_{k,m}(\rho,\lambda)\cdot e^{i(m\varphi+\lambda z)}$;

$$\tilde{\vec{b}}_{1,n}(\rho,\lambda) = \vec{e}_\rho \cdot I_n'(\lambda\rho) + i\cdot I_n(\lambda\rho)\cdot\left(\vec{e}_\varphi \frac{n}{\lambda\rho} + \vec{e}_z\right);$$

$$\tilde{\vec{b}}_{2,n}(\rho,\lambda) = \vec{e}_\rho \cdot\left[(4\nu-3)\cdot I_n'(\lambda\rho) + \lambda\rho_p I_n''(\lambda\rho)\right]$$

$$+\vec{e}_\varphi i\cdot m\left(I_n'(\lambda\rho) + \frac{4(\nu-1)}{\lambda\rho} I_n(\lambda\rho)\right) + \vec{e}_z i\lambda\rho I_n'(\lambda\rho);$$

$$\tilde{\vec{b}}_{3,n}(\rho,\lambda) = -\left[\vec{e}_\rho \cdot I_n(\lambda\rho)\frac{n}{\lambda\rho} + \vec{e}_\varphi \cdot i\cdot I_n'(\lambda\rho)\right];$$

$\vec{e}_\rho$, $\vec{e}_\varphi$, $\vec{e}_z$ – unit vectors in the cylindrical coordinate system.

- transition from solutions for cylinder number *p* to solutions for cylinder number *q*

$$\vec{S}_{k,m}(\rho_p,\varphi_p,z;\lambda) = \sum_{n=-\infty}^{\infty} \vec{b}_{k,pq}^{mn}(\rho_q)\cdot e^{i\left(n\varphi_q+\lambda z\right)}, \tag{12}$$

$k = 1,\ 2,\ 3;$

$$\vec{b}_{1,pq}^{mn}(\rho_q) = (-1)^n \tilde{K}_{m-n}(\lambda\ell_{pq})\cdot e^{i(m-n)\alpha_{pq}}\cdot\tilde{\vec{b}}_{1,n}(\rho_q,\lambda);$$

$$\vec{b}_{2,pq}^{mn}(\rho_q) = (-1)^n\left\{\tilde{K}_{m-n}(\lambda\ell_{pq})\cdot\tilde{\vec{b}}_{2,n}(\rho_q,\lambda) - \frac{\lambda}{2}\ell_{pq}\times\right.$$

$$\left.\times\left[\tilde{K}_{m-n+1}(\lambda\ell_{pq}) + \tilde{K}_{m-n-1}(\lambda\ell_{pq})\right]\cdot\tilde{\vec{b}}_{1,n}(\rho_q,\lambda)\right\}\times$$

$$\times e^{i(m-n)\alpha_{pq}};$$

$$\vec{b}_{3,pq}^{mn}(\rho_q) = (-1)^n \tilde{K}_{m-n}(\lambda\ell_{pq})\cdot e^{i(m-n)\alpha_{pq}}\cdot\tilde{\vec{b}}_{3,n}(\rho_q,\lambda);$$

where α_{pq} is the angle between the axis x_p and the segment ℓ_{qp} ; $\tilde{K}_m(x) = \left(sign(x)\right)^m \cdot K_m(|x|)$.

Satisfying the boundary conditions (2)–(5) on the flat boundaries y = ±h and conditions (6) on the cavity surfaces $\rho_p = R_p$ using addition theorems (10)–(12) reduces the boundary value problem to an infinite system of linear algebraic equations with respect to the unknown amplitude functions $B_{k,m}^{(p)}(\lambda)$:

$$B_{k,m}^{(p)}(\lambda) + \sum_{q=1}^{N}\sum_{m=-\infty}^{\infty}\sum_{k=1}^{3} C_{j,n,k,m}^{(pq)}(\lambda) B_{k,m}^{(q)}(\lambda) = F_{j,n}^{(p)}, \tag{13}$$

where $\sum_{k=1}^{3} C_{j,n,k,m}^{(pq)}(\lambda)$ are the system kernels expressed via addition theorems and problem characteristics; $F_{j,n}^{(p)}$ are the right-hand sides determined by the prescribed displacements

The resulting system (13) is a regular infinite system of the second kind, which guarantees the convergence of the reduction method. The system is truncated to a finite order $n = -M, \ldots, M$, which ensures the necessary accuracy of calculations. The found amplitude functions are substituted into expression (9) to determine the full field of displacements, and then — through Hook's

law — the field of stresses in the entire volume of the layer.

2.3. Numerical studies of the stress state and discussion

Before conducting the main numerical studies, verification of the developed methodology was performed by comparison with known special cases. First, when moving to an infinite layer ($z \to \infty$) and one cavity ($N = 1$), the obtained results coincide with the solution of work [11], where the second fundamental problem of elasticity theory for a layer with a cylindrical cavity under prescribed displacements is considered. Second, in the absence of cylindrical cavities, the obtained displacement fields on the plane $z = 0$ reproduce the solution of work [21] for a half-space-shell. In all verified cases, the discrepancy between the results does not exceed 0.1%, which confirms the correctness of the developed methodology.

Numerical results were obtained for a layer made of ABS-plastic with three cylindrical cavities. Physico-mechanical characteristics of the layer: Poisson's ratio $\nu_0 = 0.38$, Young's modulus $E_0 = 1700$ MPa.

Geometric parameters of the model: $h = \tilde{h} = 10$ mm, cavities with radii $R_p = 5$ mm are located on one horizontal line $y = 0$, distances between cavities $\ell_{12} = \ell_{13} = 20$ mm.

On the horizontal boundaries of the layer $y = \pm h$ and on the surfaces of the cavities $\rho_p = R_p$, displacements are prescribed. All components not explicitly stated equal zero. Four loading variants are considered that correspond to different combinations of parity of displacement functions with respect to the coordinate z.

Variant 1. On the horizontal boundaries of the layer, a normal displacement that is an even function in z is prescribed:

$$U_y^{(h)}(x,z) = \begin{cases} -10^4 \cdot \left(x^2 + 10^2\right)^{-2}, -20 \le z \le 20; \\ 0, |z| > 20. \end{cases}$$

Variant 2. On the horizontal boundaries of the layer, a tangential displacement that is an even function in z is prescribed:

$$U_x^{(h)}(x,z) = \begin{cases} -10^4 \cdot \left(x^2 + 10^2\right)^{-2}, -20 \le z \le 20 \\ 0, |z| > 20 \end{cases}$$

Variant 3. On the horizontal boundaries of the layer, a normal displacement that is an odd function in z is prescribed:

$$U_y^{(h)}(x,z) = \begin{cases} -10^4 \cdot \left(x^2 + 10^2\right)^{-2}, 0 < z \le 20 \\ 10^4 \cdot \left(x^2 + 10^2\right)^{-2}, -20 \le z < 0 \\ 0, |z| > 20 \end{cases}$$

Variant 4. On the horizontal boundaries of the layer, a tangential displacement that is an odd function in z is prescribed:

$$U_x^{(h)}(x,z) = \begin{cases} -10^4 \cdot \left(x^2 + 10^2\right)^{-2}, 0 < z \le 20 \\ 10^4 \cdot \left(x^2 + 10^2\right)^{-2}, -20 \le z < 0 . \\ 0, |z| > 20 \end{cases}$$

In order to avoid stress singularity caused by a discontinuity of the first kind, the prescribed displacement function is smoothed in the vicinity of the points $z = \pm 20$ mm: the transition from non-zero values to zero is carried out not abruptly, but smoothly over a small interval, which corresponds to a trapezoidal approximation of the function's support.

Variants 1 and 2 correspond to loads that are even in z and model the "smooth wall" condition on the vertical end $z = 0$. On this plane, the following conditions are automatically satisfied: the normal displacement $U_z^{(z=0)}$ and tangential stresses $\tau_{xz}^{(z=0)}$, $\tau_{yz}^{(z=0)}$ are equal to zero; meanwhile, the displacements $U_x^{(z=0)}$, $U_y^{(z=0)}$, normal and tangential stresses $\sigma_y^{(z=0)}$, $\sigma_x^{(z=0)}$, $\sigma_z^{(z=0)}$, $\tau_{xy}^{(z=0)}$ are non-zero.

Variants 3 and 4 correspond to loads that are odd in z and model the "free end" condition on the plane $z = 0$. In this case, the following conditions are automatically satisfied: $U_x^{(z=0)} = U_y^{(z=0)} = 0$ and $\sigma_x^{(z=0)} = \sigma_y^{(z=0)} = \sigma_z^{(z=0)} = \tau_{xy}^{(z=0)} = 0$; meanwhile, the normal displacement $U_z^{(z=0)}$ and tangential stresses $\tau_{xy}^{(z=0)}$, $\tau_{yz}^{(z=0)}$ are not equal to zero.

On the surfaces of the cylindrical cavities, zero displacements are prescribed. The accuracy of the numerical solution of the infinite system (13) was controlled by the reduction method by increasing the truncation order M, results were considered converged at a relative error not exceeding 0.1%.

Fig. 2 shows the stress distribution on the upper boundary of the layer ($y = h$) along the z-axis for loading variants 1 and 2, which correspond to displacement functions that are even in z (the "smooth wall" condition).

ISSN 1814-4225 (print)
ISSN 2663-2012 (online)

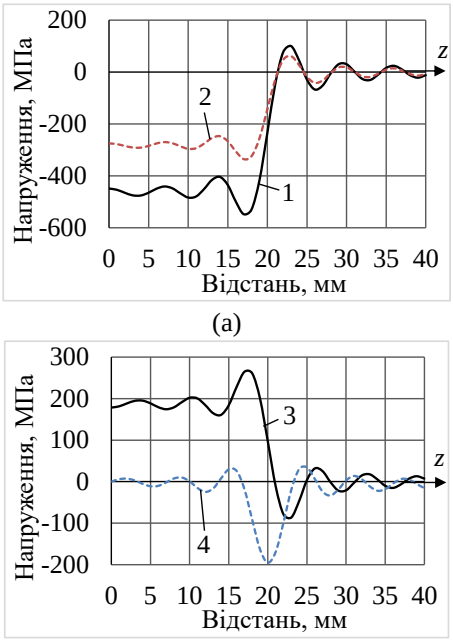

Fig. 2. Stress state on the upper surface of the layer: (a) – variant 1; (b) – variant 2; 1 – stress σ_y; 2 – stress σ_x; 3 – stress τ_{xy}; 4 – stress τ_{xz}

For variant 1 (Fig. 2(a)), where normal displacement is prescribed on the layer boundaries, the dominant component is the normal stress σ_y (curve 1), which reaches a maximum absolute value of 548 MPa in the zone $z \approx 17$ mm, which directly corresponds to the boundary of the support of the prescribed displacement. The normal stress σ_x (curve 2) is significantly smaller in magnitude. The normal stress σ_z practically coincides with σ_x, so it is not shown in Fig. 2(a). All other stress components are zero, which confirms the correctness of the implementation of the "smooth wall" condition: $\tau_{xz} = \tau_{yz} = 0$.

For variant 2 (Fig. 2(b)), where tangential displacement $U_x^{(h)}$ is prescribed, the dominant component is the tangential stress τ_{xy} (curve 3), which reaches a value of 264 MPa. The tangential stress τ_{xz} (curve 4) has the opposite sign and a smaller maximum absolute value — 195 MPa. Both components are localized in the zone $z \approx 17$–20 mm and rapidly decay to zero as the distance from this zone increases. All normal stresses are zero.

In both variants, a characteristic oscillatory stress behavior is observed with gradual decay at $z > 25$ mm. The nature of these oscillations is related to the near - jump discontinuity of the first kind of the prescribed displacement functions at $z = 20$ mm — at the point of sharp transition from non-zero load to zero. A step-like change in the boundary displacement causes a local stress concentration in the zone $z \approx 20$ mm, which propagates in the form of decaying spatial waves along the axis z. Increasing the reduction order of the system does not eliminate these oscillations, which confirms their physical nature: they are an inherent response of an elastic body to a sharp loading transition. At $z > 30$ mm, the stresses are practically equal to zero in both variants, indicating the local nature of this effect.

Fig. 3 shows the stress distribution on the upper boundary of the layer ($y = h$) along the axis z for loading variants 3 and 4, which correspond to displacement functions that are odd in z (the "free end" condition).

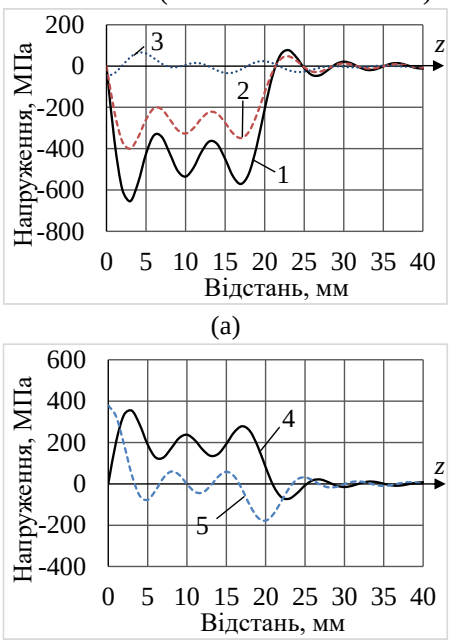

Fig. 3. Stress state on the upper surface of the layer: a – variant 3; b – variant 4; 1 – stress σ_y; 2 – stress σ_x; 3 – stress τ_{yz}; 4 – stress τ_{xy}; 5 – stress τ_{xz}

For variant 3 (Fig. 3(a)), where odd normal displacement $U_y^{(h)}$ is prescribed, the dominant component is the normal stress σ_y (curve 1), which reaches a maximum absolute value of 654 MPa — noticeably higher than in variant 1. The normal stress σ_x (curve 2) is smaller in magnitude and also has an oscillatory character with a maximum of 400 MPa. The normal stress σ_z practically coincides with σ_x and is not shown in Fig. 3(a). The tangential stress τ_{yz} (curve 3) is small compared to the normal components. All other stress components are zero. It should be noted that, unlike variant 1, where the load is even in z and the stresses have one pronounced extremum near $z = 20$ mm, in variant 3, the oddness of the load causes the appearance of a stress concentration directly near the vertical end (at $z = 0$), where the prescribed displacement undergoes the largest sign-change gradient.

For variant 4 (Fig. 3b), where an odd tangential displacement $U_x^{(h)}$ is prescribed, the dominant component is the tangential stress τ_{xy} (curve 4), reaching a value of about 354 MPa near $z = 0$ and gradually decaying at $z >$ 25 mm. The tangential stress τ_{xz} (curve 5) has a maximum

value of 379 MPa directly at the vertical end ($z = 0$). All normal stresses are zero.

Comparing variants 3 and 4 with variants 1 and 2, the following observations can be made. First, odd loads (variants 3, 4) generate higher maximum stresses: σ_y increases by approximately 23%, and τ_{xy} — by 35%. Second, for odd loads, the stress concentration zone shifts toward the end $z = 0$, whereas for even loads, it is localized near $z = 20$ mm — at the point of discontinuity of the prescribed displacements. Third, the oscillatory nature of the stress distribution is a common feature of all four variants and is caused by the sharp transition of the prescribed displacements from non-zero values to zero.

Fig. 4 shows the stress distribution on the surface of the most loaded cylindrical cavity $p = 1$ with respect to the rotation angle $\varphi \in [0, 2\pi]$ for loading variants 1 and 2 (displacements even in z, the "smooth wall" condition).

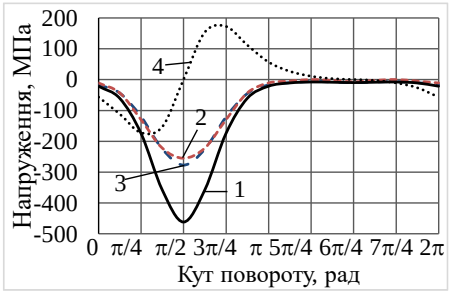

(a)

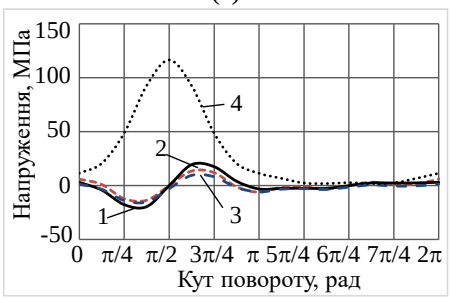

(b)

Fig. 4. Stress state on the upper surface of the layer: a – variant 1; b – variant 2; 1 – stress σ_ρ; 2 – stress σ_φ; 3 – stress σ_z; 4 – stress $\tau_{\rho\varphi}$

For variant 1 (Fig. 4(a)), all stress components exhibit pronounced non-uniformity with respect to the rotation angle. The radial stress σ_ρ (curve 1) is the largest in absolute value, reaching a minimum of about −462 MPa in the zone $\varphi = \pi/2$, that is , at the point closest to the loaded upper boundary of the layer. The axial stress σ_z (curve 3) is also significant (−277 MPa) and is similar in the nature of its distribution to σ_ρ. The hoop stress σ_φ (curve 2) is smaller in magnitude with a minimum of −255 MPa. The tangential stress $\tau_{\rho\varphi}$ (curve 4) changes sign: it reaches a maximum of +172 MPa at $\varphi \approx \pi/4$ and a minimum of −172 MPa at $\varphi \approx 3\pi/4$, which corresponds to the inclined sections of the cavity surface relative to the direction of the applied load. All other stress components are zero.

For variant 2 (Fig. 4(b)), where tangential displacement $U_x^{(h)}$ is prescribed, the nature of the stress distribution is significantly different. The dominant component is the tangential stress $\tau_{\rho\varphi}$ (curve 4), which reaches a maximum of +116 MPa at $\varphi = \pi/2$. The radial stress σ_ρ (curve 1) reaches ±19.4 MPa, the hoop stress σ_φ (curve 2) is ±13.6 MPa, and σ_z (curve 3) is –15,3 MPa. All other stress components are zero.

A comparison of variants 1 and 2 indicates that normal displacement on the layer boundaries causes a significantly greater stress concentration on the cavity surface than tangential displacement: the maximum stresses in variant 1 exceed the corresponding values in variant 2 by approximately 3.5–4 times.

Fig. 5 shows the distribution of stresses on the surface of the most loaded cylindrical cavity $p = 1$ with respect to the rotation angle $\varphi \in [0, 2\pi]$ for loading variants 3 and 4 (displacements odd in z, condition of a "free end"). Unlike variants 1 and 2, only the tangential components $\tau_{\rho z}$ and $\tau_{\varphi z}$ are non-zero, which fully corresponds to the condition of a "free end" on the plane $z = 0$.

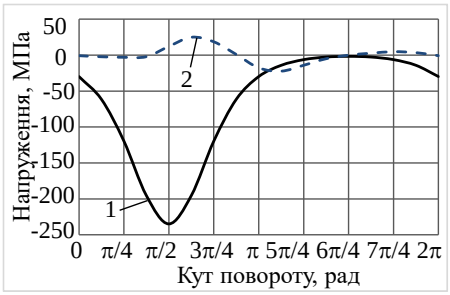

(a)

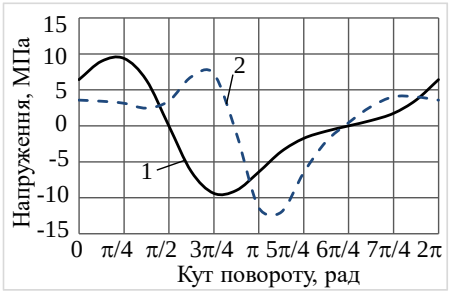

(b)

Fig. 5. Stress state on the upper surface of the layer: a – variant 3; b – variant 4; 1 – stress $\tau_{\rho z}$; 2 – stress $\tau_{\varphi z}$

For variant 3 (Fig. 5(a)), where an odd normal displacement $U_y^{(h)}$ is prescribed, the dominant component is the tangential stress $\tau_{\rho z}$ (curve 1), which reaches a minimum of −235 MPa in the zone $\varphi = \pi/2$ — that is, at the point of the cavity surface closest to the loaded layer boundary. The tangential stress $\tau_{\varphi z}$ (curve 2) is significantly smaller in absolute value, at ±25 MPa. All other

ISSN 1814-4225 (print)
ISSN 2663-2012 (online)

stress components are zero.

For variant 4 (Fig. 5(b)), where an odd tangential displacement $U_x^{(h)}$ is prescribed, both components are comparable in magnitude. The tangential stress $\tau_{\rho z}$ (curve 1) changes sign along the circumference of the cavity: it reaches a maximum of ±9.47 MPa. The tangential stress $\tau_{\varphi z}$ (curve 2) is also alternating with a maximum of +7.2 MPa at $\varphi \approx \pi/4$ and a minimum of about −12 MPa at $\varphi \approx 5\pi/4$. All other stress components are zero.

A comparison of Fig. 4 and Fig. 5 reveals a fundamental difference between the conditions of a "smooth wall" and a "free end" from the standpoint of loading of the cavity surface. Under even loads (variants 1, 2), all stress components in the plane of the cross-section (σ_ρ, σ_φ, σ_z, $\tau_{\rho\varphi}$) arise on the cavity surface with maximum values up to 462 MPa. Under odd loads (variants 3, 4), only the components $\tau_{\rho z}$ and $\tau_{\varphi z}$ are non-zero, and their level is significantly lower: maximum values do not exceed 235 MPa in variant 3 and 12 MPa in variant 4. This difference is explained by the fact that odd loads induce predominantly an antiplane stress-strain state in the cavity cross-section, whereas even loads induce a plane one.

Conclusions

In this paper, an analytical-numerical methodology has been developed for solving the spatial problem of elasticity theory for a semi-infinite isotropic layer with *N* longitudinal cylindrical cavities under prescribed displacements on all surfaces of the body. The obtained results allow for the following conclusions.

1. The application of the mirror reflection method to the problem for a semi-infinite layer with cylindrical cavities under kinematic boundary conditions is an effective approach that reduces the problem for a semi-infinite body to an equivalent problem for an infinite layer. Prescribing displacements with even or odd parity in the coordinate *z* on the horizontal boundaries of the infinite layer automatically ensures the fulfillment of the " smooth wall " or " free end " conditions on the plane $z = 0$ without directly introducing this boundary into the solution.

2. The reliability of the obtained results is confirmed by verification: in the limiting transitions to special cases — an infinite layer with one cavity [11] and a semi-infinite layer without cavities [21] — the discrepancy with known solutions does not exceed 0.1%.

3. The four considered variants of boundary conditions generate qualitatively different stress fields both on the horizontal layer boundaries and on the surfaces of the cylindrical cavities. Loads even in *z* (variants 1 and 2, condition of a "smooth wall") cause the emergence of a full set of stress components in the cavity cross-section with maximum values up to 462 MPa. Loads odd in *z* (variants 3 and 4, condition of a "free end") generate predominantly an anti-plane stress state: only the components $\tau_{\rho z}$ and $\tau_{\varphi z}$ are non-zero on the cavity surface, with significantly lower maximum values.

4. The highest stress concentration on the cavity surface is observed under the action of normal displacement on the layer boundaries (variant 1): the maximum value of σ_ρ reaches 462 MPa, which is 3.5–4 times higher than the corresponding values under tangential displacement (variant 2). This indicates the decisive role of the normal displacement component in the formation of the stress concentration around the cavity.

5. On the horizontal layer boundaries, in all four variants, an oscillatory stress distribution is observed, localized near the point of discontinuity of the prescribed displacements ($z = 20$ mm) or near the vertical end ($z = 0$). The oscillations have a physical nature — they are the response of an elastic body to a sharp loading transition from non-zero values to zero, which is confirmed by their independence from the reduction order of the system.

6. Odd loads (variants 3 and 4) form higher levels of normal stresses on the horizontal layer boundaries compared with the corresponding even variants: the maximum of σ_y increases from 548 MPa (variant 1) to 654 MPa (variant 3), and the maximum of τ_{xy} — from 264 MPa (variant 2) to 354 MPa (variant 4). This is explained by the shift of the concentration zone toward the vertical end $z = 0$, where the "free end" condition does not limit the development of deformations in the plane of the end.

7. The developed methodology is general and can be applied to an arbitrary number *N* of cylindrical cavities with different radii and locations in the layer cross-section, as well as to other isotropic materials. The obtained results can serve as a benchmark for the verification of numerical methods of calculation (FEM) in the analysis of structures with cylindrical channels undergoing forced deformation.

Conflict of Interest

The authors declare that they have no conflict of interest in relation to this research, whether financial, personal, author ship or otherwise, that could affect the research and its results presented in this paper.

Financing

This study was conducted without financial support.

Data Availability

The manuscript has no associated data.

Use of Artificial Intelligence

The author confirm that he did not use artificial intelligence methods while creating the presented work.

The author had read and agreed to the published version of this manuscript.

References

1. Savin, G. N. *Stress Concentration Around Holes*. Oxford, London, New York, Paris, Pergamon Press, 1961. 430 p.
2. Kosmodamianskiy, A. S. *Teoreticheskaya i prikladnaya mekhanika* [Theoretical and applied mechanics]. Donetsk, Donets. nats. un-t Publ., 2001. 140 p. (In Russian).
3. Podilchuk, Yu. N. *Trekhmernye zadachi teorii uprugosti* [Three-dimensional problems of the theory of elasticity]. Kyiv, Naukova dumka Publ., 1979. 440 p. (In Russian).
4. Grinchenko, V. T., Meleshko, V. V. *Garmonicheskie kolebaniya i volny v uprugikh telakh* [Harmonic vibrations and waves in elastic bodies]. Kyiv, Naukova dumka Publ., 1981. 472 p. (In Russian).
5. Tekkaya, A. E., Soyarslan, C. Finite element method. *CIRP Encyclopedia of Production Engineering*, Springer Berlin Heidelberg, 2014, pp. 508–514. DOI: https://doi.org/10.1007/978-3-642-20617-7_16699.
6. *Static structural simulation using Ansys Discovery*. Available at: https://courses.ansys.com/index.php/courses/structural-simulation (accessed 09 June 2026).
7. Nikolaev, A. G., Protsenko, V. S. *Obobshchennyy metod Fure v prostranstvennykh zadachakh teorii uprugosti* [Generalized Fourier method in spatial problems of the theory of elasticity]. Kharkiv, Nats. aerokosm. un-t «KhAI» Publ., 2011. 432 p. (In Russian).
8. Fesenko, A., Vaysfel'd, N. The wave field of a layer with a cylindrical cavity in structural integrity. *Structural Integrity*, Springer International Publishing, 2019, pp. 277–282. DOI: https://doi.org/10.1007/978-3-030-21894-2_51.
9. Fesenko, A., Vaysfel'd, N. The dynamical problem for the infinite elastic layer with a cylindrical cavity. *Procedia Structural Integrity*, 2021, vol. 33, pp. 509–527. DOI: https://doi.org/10.1016/j.prostr.2021.10.058.
10. Khechai, A., Belarbi, M. O., Bouaziz, A., Rekbi, F. M. L. A general analytical solution of stresses around circular holes in functionally graded plates under various in-plane loading conditions. *Acta Mechanica*, 2023, vol. 234, pp. 671–691. DOI: https://doi.org/10.1007/s00707-022-03413-1.
11. Miroshnikov, V. Yu. The study of the second main problem of the theory of elasticity for a layer with a cylindrical cavity. *Strength of Materials and Theory of Structures*, 2019, no. 102, pp. 77–90. DOI: https://doi.org/10.32347/2410-2547.2019.102.77-90.
12. Miroshnikov, V., Younis, B., Savin, O., Sobol, V. A linear elasticity theory to analyze the stress state of an infinite layer with a cylindrical cavity under periodic load. *Computation*, 2022, vol. 10, no. 9, article no. 160. DOI: https://doi.org/10.3309/computation10090160.
13. Nikichanov, V. V. Determination of the stress state of a layer with a cylindrical cavity under given smooth contact conditions on the layer boundaries and displacements on the cavity surface. *Proceedings of the 9th International Scientific and Practical Conference "Scientific Horizon in the Context of Social Crises"*, Otsuki Press, 2021, pp. 208–213. Available at: https://ojs.ukrlogos.in.ua/index.php/interconf/issue/view/6-8.08.2021/569 (accessed 10 April 2022).
14. Miroshnikov, V., Savin, O., Sobol, V., Nikichanov, V. Solving the problem of elasticity for a layer with N cylindrical embedded supports. *Computation*, 2023, vol. 11, no. 9, article no. 172. DOI: https://doi.org/10.3309/computation11090172.
15. Vitaly, M. Rotation of the layer with the cylindrical pipe around the rigid cylinder. *CAMPE 2021: Advances in Mechanical and Power Engineering*, Springer, 2023, pp. 314–322. DOI: https://doi.org/10.1007/978-3-031-18487-1_32.
16. Sverdlov, S. Determination of the stress-strain state of a bearing connection. *Proceedings of the 2nd International Scientific and Practical Conference "Modern Trends in the Development of Economy, Technology and Industry"*, International Scientific Unity, 2025, pp. 229–233. Available at: https://isu-conference.com/en/archive/modern-trends-in-the-development-of-economy-technology-and-industry-12-02-25/ (accessed 15 February 2025).
17. Denshchykov, O. Y. First main problem of the theory of elasticity for a layer with two thick-walled pipes and one cylindrical cavity. *Journal of Mechanical Engineering*, 2025, vol. 28, no. 2, pp. 44–53. DOI: https://doi.org/10.15407/pmach2025.02.044.
18. Kosenko, M. Solution to an elasticity problem for a layer with cylindrical embedded supports in the form of a cavity and a pipe: Rigid fixation. *Proceedings of the Interdisciplinary Scientific and Practical Conference "Modern Problems of the Development of the Aerospace Industry of Ukraine: Engineering, Business, Law"*, 2024, pp. 170–174.
19. Ilin, O., Kosenko, M., Denshchykov, O. Analysis of the stress state of a reinforced layer with two cylindrical cavities and some contact-type conditions. *Colloquium-Journal*, 2024, no. 19, pp. 8–13. DOI: https://doi.org/10.5281/zenodo.12723815.
20. Arkhypenko, I. O., Savin, O. B. Kontseptsiia rozviazannia zadachi teorii pruzhnosti dlia napivneskinchenoho sharu [Concept of solving the problem of elasticity theory for a semi-infinite layer]. *Theses of 5th International Scientific and Practical Conference "Global Trends in the Development of Information Technology and Science"*, 2025, pp. 346–348. Available at: https://isu-conference.com/wp-content/uploads/2025/01/Sweden_1_08.01.2025.pdf (In Ukrainian).
21. Arkhypenko, I. O., Savin, O. B. Solution of the spatial problem of elasticity theory for a half-space shell. *Colloquium-Journal*, 2025, vol. 60, no. 253, pp. 3–6. DOI: https://doi.org/10.5281/zenodo.17013675.
22. Arkhypenko, I., Sverdlov, S., Ilin, O., Miroshnikov, V., Fomichev, P. Stress state analysis of semi-infinite layer with cylindrical hinged joint. *International Science Journal of Engineering & Agriculture*, 2026, vol. 5, no. 2, pp. 65–80. DOI: https://doi.org/10.46299/j.isjea.20260502.07.

ISSN 1814-4225 (print)
ISSN 2663-2012 (online)

Received 09.05.2026, Received in revised form 09.06.2026
Accepted date 15.06.2026, Published date 17.06.2026

АНАЛІЗ НАПРУЖЕНОГО СТАНУ НАПІВОБМЕЖЕНОГО ШАРУ З ЦИЛІНДРИЧНИМИ ПОРОЖНИНАМИ

І. О. Архипенко

Предметом статті є напружено-деформований стан напівобмеженого ізотропного пружного шару з N поздовжніми циліндричними порожнинами за заданих переміщень на всіх поверхнях тіла. **Метою є** розробка аналітико-чисельної методології розв'язання просторової задачі пружності для напівобмеженого шару з циліндричними порожнинами за кінематичних граничних умов та дослідження напруженого стану для чотирьох якісно різних варіантів граничних умов, що відрізняються парністю заданих компонент переміщень відносно координати z. **Задачі**, що потребують вирішення, такі: побудувати розв'язок рівнянь Ламе в декартовій та локальній циліндричній системах координат; звести задачу для напівобмеженого шару до еквівалентної задачі для нескінченного шару; задовольнити граничні умови на всіх поверхнях та звести задачу до нескінченної системи лінійних алгебраїчних рівнянь; отримати числові розподіли напружень на межах шарів та поверхнях порожнин; перевірити методологію на відомих розв'язках. **Використані методи**: узагальнений метод Фур'є з теоремами додавання для переходу між системами координат; метод дзеркального відбиття, за допомогою якого призначення парних або непарних переміщень на горизонтальних межах автоматично забезпечує умови «гладкої стінки» або «вільної грані» на площині $z = 0$; та метод редукції для розв'язання результуючої нескінченної системи лінійних алгебраїчних рівнянь другого роду. **Висновки**. Парні навантаження призводять до майже повного набору компонентів напружень у поперечному перерізі порожнини, тоді як непарні навантаження створюють переважно антиплощий напружений стан. Нормальне зміщення призводить до концентрації напружень на поверхні порожнини, яка в 3,5–4 рази перевищує тангенціальне зміщення тієї ж амплітуди. Коливальний розподіл напружень поблизу точок розриву заданих переміщень має фізичну природу та не залежить від порядку усічення системи. **Наукова новизна**. Вперше розв'язано задачу просторової пружності для напівобмеженого шару з N циліндричними порожнинами за кінематичних граничних умов. Поєднання узагальненого методу Фур'є з методом дзеркального відбиття поширено на напівобмежене тіло з циліндричними неоднорідностями. Методологія застосовна до довільної кількості порожнин і може служити еталоном для перевірки розрахунків методом скінченних елементів.
Ключові слова: напівобмежений шар; циліндрична порожнина; кінематичні граничні умови; узагальнений метод Фур’є; напружено-деформований стан; просторовий крайовий ефект.

Архипенко Ігор Олексійович – аспірант каф. Міцності літальних апаратів, Національний аерокосмічний університет «Харківський авіаційний інститут», Харків, Україна.

Ihor Arkhypenko – Postgraduate Student of the Department of Aircraft Structural Strength, National Aerospace University “Kharkiv Aviation Institute,” Kharkiv, Ukraine,
e-mail: i.o.arkhypenko@khai.edu, ORCID: 0009-0009-0311-4437.